

**NASA TECHNICAL  
MEMORANDUM**

NASA TM X- 67979

NASA TM X- 67979

**CASE FILE  
COPY**

**PEAK AXIAL-VELOCITY DECAY WITH SINGLE-  
AND MULTI-ELEMENT NOZZLES**

by U. H. von Glahn, D. E. Groesbeck, and R. G. Huff  
Lewis Research Center  
Cleveland, Ohio

TECHNICAL PAPER proposed for presentation at  
Tenth Aerospace Sciences Meeting sponsored by the  
American Institute of Aeronautics and Astronautics  
San Diego, California, January 17-19, 1972

# PEAK AXIAL-VELOCITY DECAY WITH SINGLE- AND MULTI-ELEMENT NOZZLES

by U. H. von Glahn, D. E. Groesbeck, and R. G. Huff  
National Aeronautics and Space Administration  
Lewis Research Center  
Cleveland, Ohio

## Abstract

Jet peak-velocity decay data were obtained for a variety of circular and noncircular single-element and multi-element nozzles for application to externally-blown-flap STOL aircraft. These data permit a rational approach, in terms of element type and element spacing, to nozzles designed to promote mixing of the jet exhaust with the surrounding air. Rapid mixing and the resulting lower axial jet velocity decreases the noise caused by the interaction of jet impingement on the flap assembly of EBF STOL aircraft. Empirical relationships are presented that permit the prediction of peak axial-velocity decay curves for a wide spectrum of mixer-type nozzles. The data are useful also in the design of ejector-type noise suppressors and for the suppression of VTOL downwash velocities caused by vertically oriented exhaust nozzles.

## Introduction

The air transportation system of the 1980's is expected to include substantial numbers of STOL aircraft. Of the several lift augmentation concepts proposed for STOL aircraft, the present study is concerned with externally blown flaps (fig. 1). Experimental studies have shown that the impingement of the engine exhaust jet on deflected flaps can cause an unacceptable increase in the aircraft noise signature.<sup>(1-3)</sup> The increase in noise level is a 6-power function of the impinging jet velocity on the flap surfaces<sup>(1)</sup> and is also proportional to the surface area scrubbed by the jet. The jet-flap interaction noise can be lowered by reducing the impinging velocity on the flap.<sup>(1,2)</sup> This velocity reduction generally must be accomplished in a specified distance from the jet exhaust plane to the flap.

The jet velocity impinging on the flap can be reduced by: (1) a reduction of the jet velocity at the exhaust by utilizing a large bypass-type fan engine and (2) by use of a mixer-type nozzle, consisting of multi-elements rather than a single large exhaust nozzle of equal total area. The individual small elements of a mixer nozzle promote an initially rapid mixing with the surrounding air resulting in a rapid axial velocity decay.

It is the purpose of this paper to summarize the results of an experimental study,<sup>(4)</sup> conducted at the NASA Lewis Research Center, on the peak axial-velocity decay obtained with circular and noncircular single-element nozzles and several multi-element mixer nozzles. Empirical equations are developed for estimating peak axial-velocity decay curves for a wide range of nozzle configurations.

## Apparatus

### Test Stand

The test stand used in the present work is

shown in figure 2. Pressurized air at about 289 K is supplied to a 15.25-cm diameter plenum by twin diametrically opposed supply lines. Flexible couplings in each of the twin supply lines isolate the supply system from a force measuring system. In the present study no thrust measurements were used. The test nozzles were attached to a flange at the downstream end of the plenum.

Airflow through the overhead main supply line was measured with a calibrated orifice. The nominal nozzle inlet total pressure was measured with a single probe near the plenum exit flange.

Free jet surveys were made with a traversing pitot-static probe at several downstream stations (up to about 50-cm) from the test nozzle exit planes. Thereafter, a single pitot-static probe located on the approximate centerline of the nozzle was used at downstream distances up to 300 cm.

The measurements from the traversing probe were transmitted to an x-y-y' plotter which yielded direct traces on graph paper of the total and static pressure distribution radially across the jet. All other pressure data were recorded from multitube water or mercury manometers.

## Nozzles

Peak axial velocity degradation data were obtained with single-element nozzles that included the following cross sections: circular, trapezoidal, triangular, and rectangular. The studies included variations in nozzle aspect ratio and nozzle area.

Multi-element nozzles included multitubes (up to 19 tubes) and multi-lobe nozzles (up to 12 lobes). The spacing between elements and circumferential rings of elements (for multitube nozzles) were studied to evaluate these geometry effects on peak axial-velocity degradation.

## Procedure

Initially, the traversing probe was positioned 0.317-cm from the nozzle exit plane and radial pressure-traverses were made in the plane of the largest element dimension (i.e., diameter of a circular element, width of a rectangular element, etc.). Pressure measurements were obtained at nominal nozzle pressure ratios of 1.15, 1.31, 1.53, 1.87, and 2.3. This procedure was then repeated at nominal distances from the nozzle exit plane of 13-, 25-, 38-, and 51-cm. At the same time a single pitot-static probe was moved manually to various locations from 100- to 300-cm downstream from the nozzle exit plane and pressure data recorded.

## Results and Discussion

### General

According to the literature,<sup>(5,6)</sup> the peak

axial velocity decay,  $U/U_j$ , downstream of the jet core varies as a function of  $X^{-1}$  for circular nozzles to  $X^{-1/2}$  for infinite or large aspect ratio rectangular (slot) nozzles. (All symbols are defined in the appendix.) For other single element geometries the decay appears to vary between these exponents. The axial distance is non-dimensionalized by the effective diameter of the element; i.e.,  $X/D_e$ .

For multi-element nozzles, the initial peak axial-velocity decay (fig. 3) is substantially the same as that for an individual element. However, at some distance downstream of the nozzle exit plane, the individual jets coalesce sufficiently to form a large diameter coalescing core and a very slow peak-velocity decay occurs. Once the coalesced core has fully formed, normal mixing again occurs with an associated rapid velocity decay. The literature<sup>(7,8)</sup> nondimensionalizes the multi-element nozzle decay distance by use of an effective diameter based on the total nozzle exhaust area. However, from the wide range of configuration variables covered herein, it was determined that the effective diameter of a single-element was more useful for correlation purposes and practical applications.

The peak velocity ratio,  $U/U_j$ , at a given axial station has been found to increase with increasing jet Mach number.<sup>(7,8)</sup> In general, correlation of the jet Mach number was achieved by dividing the axial distance parameter,  $X/D_e$ , by  $\sqrt{1 + M_j}$ . Data for representative single-element (conical convergent nozzle) and multi-element (multitube nozzle) configurations are shown in figure 4 using the  $\sqrt{1 + M_j}$  factor to correlate variations in  $M_j$ . The Mach number correlation factor for the multitube nozzle applies to the entire decay curve including the coalescing core and coalesced core regions. In order to avoid confusing subsequent figures with a large number of data points, hereinafter only the nominal 0.99 jet Mach number data, unless specifically noted, will be shown.

The following sections will present decay data for a variety of single-element nozzles and multi-element configurations together with correlating equations. Typical radial profile of velocity ratio at the point of departure of the coalescing core from the single element curve also will be shown and the jet spreading angle will be discussed briefly.

#### Single-Element Nozzles

Four basic single-element nozzle types were studied in order to provide sufficient information for establishing correlation equations on which to base multi-element mixer nozzle designs. These basic nozzles consisted of circular, rectangular, trapezoidal, and triangular cross-sections. It was established early in the program that the location of a baseplate at the nozzle exhaust plane did not affect the peak axial-velocity decay of single-element jets. Consequently, many of the single-element configurations were simple orifice-type nozzles rather than tubular-type nozzles.

Circular nozzles. The peak axial-velocity decay data for a conical convergent nozzle (7.63-cm I.D.<sup>(7)</sup>) were used as a standard for comparison of the present tube (2.36-cm I.D., 10-cm long) and

circular orifice data (2.46-cm I.D.) obtained in the present study. The velocity decay data for these configurations are shown in figure 5 in terms of the ratio of the local peak velocity to the jet exhaust velocity,  $U/U_j$ , as a function of the decay distance parameter  $X(C_n D_e \sqrt{1 + M_j})^{-1}$ . It is apparent that the velocity decay data for all four nozzle types are identical when an appropriate nozzle coefficient,  $C_n$ , is used. This coefficient is a function of three variables:

- (1) The ratio of the measured mass flow to the calculated ideal mass flow.
- (2) An entrance factor including a secondary dependency (<10-percent) on the number of elements used. (The latter is believed unique to the supply line and diffusers used upstream of the test nozzles in the present test rig.)
- (3) A jet Mach number correction for the orifice configurations. The overall coefficients ( $C_n$  values) are shown on the succeeding figures.

The curve shown in figure 5 is calculated from the following empirical equations:

$$\frac{U}{U_j} = \left[ 1 + \left( \frac{0.15 X}{C_n D_e \sqrt{1 + M_j}} \right)^a \right]^{-1/a} \quad (1)$$

The exponent  $a$  is a complex function of nozzle exit geometry. Over the range of nozzle geometries studied herein, the following equation, obtained by crossplotting of experimental data, provides good correlation of single-element velocity decay data:

$$a = 4 \left( 2 - (b_1/b_o) \right) \left( 1 + \frac{8}{3} (D_e/D_h - 1) \right)^{-1} \quad (2)$$

For a circular nozzle the  $a$ -exponent reduces to 4.

Rectangular nozzles. The peak axial-velocity decay data for four rectangular-orifice nozzles with aspect ratios (length/height) varying from 1.5 to 12 are shown in figure 6 together with calculated velocity decay curves. (All pertinent nozzle dimensions are summarized in table I.) In general, the data show that with increasing aspect ratio, the peak velocity initially decays more rapidly. As jet mixing with the surrounding air proceeds farther downstream from the nozzle exit plane, the velocity decay for all nozzles becomes substantially the same.

Triangular and trapezoidal nozzles. Data for single-element triangular-orifice nozzles and the trapezoidal nozzles<sup>(4)</sup> fell within the envelope of the rectangular nozzle data shown in figure 6 and are correlated well by equations (1) and (2).

#### Multi-Element Nozzles

The peak axial-velocity decay curves for several categories of multi-element nozzles, photographs of which are shown in figure 7, were determined. The first category consisted of coplanar multitube nozzles including single and multiple rings of tubes, the second consisted of single ring coplanar multi-lobe nozzles while the final category consisted of several specialty, non-

coplanar nozzles.

Empirical equations were developed to correlate the peak axial-velocity decay of these multi-element nozzle types in terms of the significant flow regimes shown previously in figure 3 and in terms of pertinent nozzle dimension parameters. These equations are limited by the general nozzle geometries tested; however, they are useful in predicting the decay curves for many practical nozzle configurations.

### Correlation

The decay curve was divided into several regions shown in figure 8. Equations were then developed to predict the departure point of the coalescing core from the single-element decay curve (point ①). Examination of the data showed that the velocity ratio in the coalescing core decay region had a slope of -0.2 with respect to axial distance (region denoted by ① to ②). The non-dimensional displacement parameter,  $D_x$ , of the coalesced-jet decay curve from the single-element curve was then determined. The value of  $U/U_j$  at point ② was then correlated in terms of the coalescing core decay slope and the displacement distance  $D_x$ . Finally, the correlation equation for the decay curve of the fully coalesced core was established.

Empirical equations for the preceding points and regions are given in the following paragraphs.

The departure point ① is calculated by the following equation:

$$\left( \frac{x}{C_n D_e \sqrt{1 + M_j}} \right)_{\text{①}} = Z_{\text{①}} \quad (1)$$

$$= 12 \left( 1 + \frac{1}{4} \left( \frac{s_1}{w_1} \right)^{2/3} \right) \left( \frac{s_1}{w_1} \right)^{1/3} f \left( \frac{D_e}{D_h} \right) f \left( \frac{r}{s} \right) \quad (3)$$

where

$$f \left( \frac{D_e}{D_h} \right) = \left[ 1 + \frac{2.67 \left( \frac{D_e}{D_h} - 1 \right)}{1 + 5 \left( 1 - \frac{b_i}{b_o} \right)^8} \right]^{-1} \quad (4)$$

and

$$f \left( \frac{r}{s} \right) = \left[ 1 + 0.33 \frac{r}{s} (f(w)) \left( \frac{U_s}{U_c} \right)^2 \right]^{-1} \quad (5)$$

The following table summarizes the necessary ratios of  $(r/s)$  and  $f(w)$  for use in equation (5).

Nozzle	$r/s$	$f(w)$
Center element with 1 or 2 rings of multi-elements	$r_1/s_1$	$w_1/w_0$
2 rings of multi-elements, no center element	$r_2/s_2$	$w_2/w_1$

The displacement of the fully coalesced multi-element core from the single element curve ( $D_x$  in fig. 8) is calculated from the following equation:

$$D_x = 1 + \left( \frac{A_c + A_s \left( \frac{U_s}{U_c} \right)^2}{A_e} - 1 \right) \left[ 1 + \frac{s_1}{w_1} \left( \frac{1}{1 + 50 \left( \frac{D_e}{D_h} - 1 \right)^{5/3}} \right) \right]^{-1/2} \quad (6)$$

When the  $U_s/U_c$  values are 1, the term

$$\sqrt{\frac{A_c + A_s \left( \frac{U_s}{U_c} \right)^2}{A_e}} \quad \text{in equation (6) reduces to } \frac{D_{e,T}}{D_e}$$

The velocity decay in the coalescing core (region ① to ②) is given by the following relationship:

$$\left| \frac{U}{U_j} \right|_{\text{①} \rightarrow \text{②}} = \left| \left( \frac{U}{U_j} \right)_{\text{①}} \left( \frac{Z_{\text{①}}}{x} \right)^{1/5} \right|_{\text{①} \rightarrow \text{②}} \quad (7)$$

In the coalesced core region (fig. 8) the velocity ratio is given by:

$$\left| \frac{U}{U_j} \right|_{\text{②} \rightarrow \infty} = \left| \left[ 1 + \left( \frac{0.15 x}{D_x C_n D_e \sqrt{1 + M_j}} \right)^a \right]^{-1/a} \right|_{\text{②} \rightarrow \infty} \quad (8)$$

The intersection of curves calculated from equations (7) and (8) provides the location of point ② in figure 8.

### Coplanar Multitube Nozzles

Multi-element nozzles consisting of six circular tubes (each 2.36 cm I.D. and 10.16 cm long) were studied to determine the effect of the circumferential spacing between adjacent tubes on the peak axial-velocity decay. (Pertinent nozzle dimensions and configuration code designations are given in table I. Typical data obtained with these nozzles are shown in figure 9 together with calculated decay curves. Initially, the velocity decay curve for all nozzles coincides with that for a single tube. As the circumferential spacing between the individual jets was decreased, the departure point of the coalescing-core curve from the single-tube curve occurs at increasingly larger values of  $U/U_j$  (i.e., shorter axial distances from the nozzle exit plane).

In order to accommodate larger total flows (within the requirements of achieving a required

velocity decay in a given axial distance), multiple rings of multi-elements are required. Nozzles consisting of two rings of multitubes each with 6 tubes in the inner ring and 6 and 12 tubes, respectively, in the outer ring (all tubes had an I.D. of 2.36 cm) were studied to determine the interference effects of the outer ring of multitubes on the peak axial-velocity decay. As shown in figure 10 the use of multi-rings of multi-elements caused the departure point of the coalescing core from the single element curve to occur at increasingly large values of  $U/U_j$  as the number of elements in the second ring increased (decreasing circumferential spacing ratio).

The addition of a center tube on the axis of multitube nozzles also caused a significant increase in the  $U/U_j$  value at which the coalescing core departed from the single-element curve (fig. 10). The departure point from the single element curve, however, was determined by the circumferential spacing ratio of the inner ring of tubes. The outer (second) ring of tubes did not influence the departure point (for nozzles with a center tube) provided the circumferential spacing of these tubes was equal to or greater than that for the tube spacing of the inner ring.

#### Coplanar Lobe-Type Nozzles

Two lobe-type nozzles were studied. The first type consisted of flat-ended trapezoidal tubes while the second type consisted of rounded-ended trapezoidal tubes (figs. 7(b) and (c), respectively).

Three flat-ended trapezoidal nozzles with the same total area were tested to determine the effect of element spacing and element number on the peak axial-velocity decay. Data obtained with these nozzles are shown in figure 11(a) together with the calculated velocity decay curves. It is evident from the data that, for these nozzles, doubling the number of elements while maintaining the radial height and the circumferential spacing ratio constant caused only a small increase in the  $U/U_j$  value at the departure point from the single-element curve. As would be expected, an increase in the circumferential spacing ratio from 1.0 to 3.0 (by increasing the element radial height and reducing its width) for the six-element nozzle resulted in a significantly lower  $U/U_j$  value at the departure point.

The peak axial-velocity decay for a rounded-ended trapezoidal 8-lobed nozzle is shown in figure 11(b) together with calculated velocity-decay curves. The data trends shown are similar to those for the flat-ended trapezoidal nozzles.

In order to promote a greater decay of the peak axial-velocity, alternate lobes of the 8-lobed nozzle were canted  $10^\circ$  outward from the nozzle centerline. Canting the alternate lobes caused the velocity decay to be reduced by a  $\Delta U/U_j$  of about 0.12 over that with the uncanted lobes. The analysis presented previously herein has not been extended to include the effects of lobe canting; consequently, the curve shown in figure 11(b) is estimated rather than calculated.

#### Nonplanar Multi-Element Nozzles

This section presents peak-axial velocity

decay data for several noncoplanar-type nozzles typical of high-bypass fan-jet engines in which the bypass exhaust plane is some distance upstream of the core jet exhaust plane. Such nozzles may have a difference in velocity between the two jets; consequently, the data presented herein were obtained at nominal secondary to core velocity ratios,  $U_s/U_c$ , of 0.7 and 1.0. The velocity decay data shown are presented for a nominal core-jet Mach number of 0.99.

Multitube bypass-type nozzles. The first nozzle tested consisted of 8 tubes (each 1.4-cm I.D.) for the core jet and 8 round-edge orifices (each 2.54-cm I.D. and 10.16 cm long) for the secondary jet. The core and secondary jets were aligned radially. The peak axial-velocity decay data for this configuration is shown in figure 12 together with the calculated velocity decay curves. The data analysis showed that, for the present configuration, the core jet determined the peak axial-velocity decay. Therefore, the value of  $D_e$  in the abscissa of figure 12 is that for the core tube and the axial distance,  $X$ , is measured from the exit plane of the core jet. A reduction of the jet velocity ratio,  $U_s/U_c$ , from 1.0 to 0.7 caused a decrease in  $U/U_j$  at the point of departure from the single-element curve. The nozzle was tested with and without a conical center plug between and around the core tubes. Use of the plug did not affect the departure point.

The velocity decay obtained with a 3-tube core nozzle (2.36-cm I.D. tubes, no center plug) of about equal area to that for the original 8-tube core nozzle, is also shown in figure 12 for a nominal  $U_s/U_c$  value of 0.7. The use of the smaller number of large-diameter tubes caused an increase in the  $U/U_j$  value at the departure point compared with the original 8-tube core configuration.

#### Radial Profiles of Velocity

The radial profiles of jet velocities at the departure point of the coalescing core from the single-element curve for multi-element nozzles are needed in order to calculate the jet-flap interaction noise for externally-blown-flap STOL systems. In the present study, these profiles were obtained from the jet velocity contours which, in turn, were obtained from the radial profiles of velocities measured at specified axial stations downstream of the nozzle exhaust plane. Typical profiles are shown in figure 13 in terms of  $U^*/U_j$  as a function of  $R/R_n$ . When the departure point occurs at a high value of  $U/U_j$  (fig. 13(b)) the flow characteristics of the individual elements are easily identified in the profile. On the other hand, when the departure point occurs at lower values of  $U/U_j$ , the profiles are more nearly uniform up to a jet radius ratio approaching 0.8. For considerations of STOL jet-flap interaction noise, this suggests that a larger area of the flap is scrubbed by the impinging jet from a mixer nozzle compared with that for a conventional nozzle. Since the jet-flap interaction noise is proportional to  $AU_j^6$ ,<sup>(1)</sup> the noise reduction expected from the use of a lower jet impingement velocity at the flap is not fully realized due to the smaller but opposite effect of the increased scrubbed area on noise generation.

### Spreading of Multi-Element Jet Wakes

The jet spreading half-angles for several multi-element-nozzle types are summarized in figure 14. The half-angles noted are averages for the regions indicated in the accompanying sketch of a typical velocity decay curve.

The data showed that these half-angles were a function of jet mixing (velocity decay) as illustrated by the decay curve. Initially in the single-element core region ( $U/U_j \sim 1$ ), denoted by region A in figure 14, the spreading half-angle varied from  $6^\circ$  to  $8^\circ$ . The larger angles were generally associated with those nozzles having the largest spacing between adjacent elements. As the jet velocity began to decay (region B) the jets began to fill in the center portion of the configuration resulting in a spreading half-angle of only  $1^\circ$  to  $4^\circ$ . As coalescing between adjacent jets proceeds, including the departure point of the coalescing core from the single-element curve (region C), the jet spreading half-angle increased to near  $6^\circ$ . Thereafter, region D, the angle again decreased somewhat, with values in the range of  $3^\circ$  to  $5^\circ$ .

The preceding jet-wake spreading half-angles are useful in determining the vertical distance below a wing that a jet exhaust must be located in order to avoid scrubbing the wing surface with a high velocity jet for externally-blown-flap STOL aircraft. Furthermore, these half-angle data are required in the design of ejector shrouds using multi-element mixer nozzles in order to determine when the flow fills the ejector.

### Concluding Remarks

In the use of a mixer nozzle for reducing the jet-flap interaction noise from an externally blown flap for STOL aircraft applications, not only must the effect of the reduction of the impinging velocity on the flap be considered, but also the larger jet impingement area on the flap. This increased area is caused primarily by the larger overall dimensions of the mixer-nozzle jet compared with that for a conventional circular-nozzle jet. Thus, the full jet-flap interaction noise benefits resulting from the velocity decay associated with a mixer nozzle may be significantly reduced by the larger jet impingement area.

For a given velocity decay requirement, the minimum number of elements for a multi-element nozzle appears to be obtained when the design value of  $X(C_n D_e \sqrt{1 + M_j})^{-1}$  for the nozzle is at the departure point of the coalescing core from the single element curve. This criteria could result in only a small number of elements for a given nozzle application. Although this design criteria should cause minimum internal flow losses and external drag increases, it could result in little, if any, of the jet exhaust noise suppression commonly associated with multi-element nozzles. From the point-of-view of jet exhaust noise reduction, therefore, it may be desirable to use more but smaller elements and accept some small drag increase, due to an increase in the overall nozzle size, for the aircraft cruise condition.

On the basis of the preceding brief remarks, there are obvious performance trade-offs and com-

promises that can be exercised in the design of mixer nozzles for specific applications. The empirical relationships for predicting peak velocity decay curves for jets presented herein are an important step in establishing rational design procedures for mixer nozzles. Use of present technology for predicting internal nozzle-flow losses and aerodynamic penalties associated with the larger mixer-nozzle surfaces and cross-sectional profile can provide the additional necessary information to achieve optimum mixer nozzle configurations.

### Symbols

$A_c$	area of core nozzle, $\text{cm}^2$
$A_e$	area of single element, $\text{cm}^2$
$A_s$	area of bypass nozzle, $\text{cm}^2$
$b, h, L, \ell, R, r, s, w$	nozzle dimensions (see Table I), cm
$C_n$	effective nozzle (or orifice) coefficient
$D_e$	effective diameter of circular nozzle with exit area equal to that of non-circular single element ( $D_e$ for a circular nozzle equals the nozzle diameter), cm
$D_{e,T}$	effective diameter of circular nozzle with exit area equal to that of total multi-element nozzle area, cm
$D_h$	hydraulic diameter of nozzle element, cm
$D_x$	analytical displacement parameter
$M_j$	jet Mach number
$R_n$	overall nozzle radius, cm
$s/w, r/w$	ratio of effective spacing between adjacent jets (including nozzle wall thickness) at nozzle exit plane to effective element width (see table I)
$U$	local peak axial-velocity of jet, m/sec
$U^*$	local jet velocity, m/sec
$U_j$	jet exhaust velocity, m/sec
$U_s/U_c$	ratio of bypass jet velocity to core jet velocity
$X$	axial distance downstream of effective nozzle exit plane, <u>cm</u>
Subscripts:	
$i$	inner
$n$	nozzle
$o$	outer
$0$	center tube

- 1 first ring of multi-elements
- 2 second ring of multi-elements

#### REFERENCES

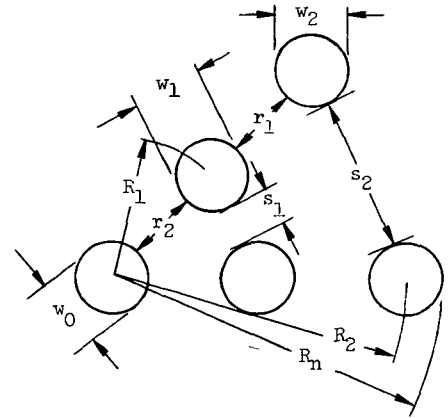
1. Dorsch, R. G., Krejsa, E. A. and Olsen, W. A., "Blown Flap Research," TM X-67850, 1971, NASA, Cleveland, Ohio.
2. Kramer, J. J., Chestnutt, D., Krejsa, E. A., Lucas, J. G., and Rice, E. J., "Noise Reduction," Aircraft Propulsion, SP-259, 1971, NASA, Washington, D.C., pp. 169-209.
3. Goodykoontz, J. H., Olsen, W. A. and Dorsch, R. G., "Preliminary Tests of the Mixer Nozzle Concept for Reducing Blown Flap Noise," TM X-67938, 1971, NASA, Cleveland, Ohio.
4. Groesbeck, D., Huff, R. and von Glahn, U., "Peak Axial-Velocity Decay with Mixer-Type Exhaust Nozzles," TM X-67934, 1971, NASA, Cleveland, Ohio.
5. Landis, F. and Shapiro, A. H., "The Turbulent Mixing of Co-Axial Gas Jets," Proceedings of Heat Transfer and Fluid Mechanics Institute, Stanford University Press, Stanford, Calif., 1951, pp. 133-146.
6. Weinstein, A. S., Osterle, J. F. and Forstall, W., "Momentum Diffusion From a Slot Jet Into a Moving Secondary," Journal of Applied Mechanics, Vol. 23, No. 3, Sept. 1956, pp. 437-443.
7. Higgins, C. C. and Wainwright, T. W., "Dynamic Pressure and Thrust Characteristics of Cold Jets Discharging from Several Exhaust Nozzles Designed for VTOL Downwash Suppression," TN D-2263, 1964, NASA, Washington, D.C.
8. Higgins, C. C., Kelly, D. P. and Wainwright, T. W., "Exhaust Jet Wake and Thrust Characteristics of Several Nozzles Designed for VTOL Downwash Suppression," CR-373, 1966, NASA, Washington, D.C.

TABLE I NOMINAL NOZZLE DIMENSIONS

Circular Tube-Type Nozzles  
(Tube I.D., 2.36 cm)

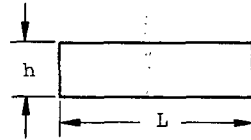
Nozzle type	$D_{e,T}$ , cm	$R_1$ , cm	$R_2$ , cm	$R_n$ , cm	$s_1/w_1$	$s_2/w_2$	$r_1/w_1$	$r_2/w_1$
0-6-0*	5.79	3.18	-----	4.35	0.344	-----	-----	-----
↓	↓	3.81	-----	5.00	.615	-----	-----	-----
		5.08	-----	6.27	1.15	-----	-----	-----
		6.67	-----	7.84	1.83	-----	-----	-----
0-6-6	8.20	5.08	10.2	11.4	1.15	3.3	-----	1.15
0-6-12	10.0	5.08	10.2	11.4	1.15	1.25	-----	1.15
1-6-0	6.25	5.08	-----	6.27	1.15	-----	1.14	-----
1-6-6	8.5	3.18	6.35	7.55	.344	1.69	.344	.344
1-6-6	8.5	5.04	10.2	11.4	1.15	3.3	1.15	1.15
1-6-12	10.3	5.04	10.2	11.4	1.15	1.25	1.15	1.15

\* Multitube nozzle designations: first number indicates if center tube is used, second number indicates number of tubes in the first ring and third number indicates number of tubes in the second ring.



Rectangular Nozzles

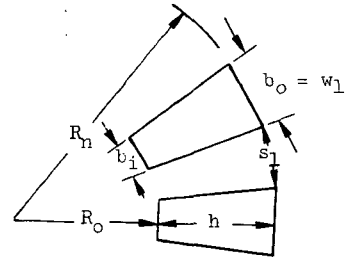
Aspect ratio	Height, h, cm	Length, L, cm
12	1.27	15.25
6	2.54	↓
3	5.08	
1.5	5.08	7.62



Trapezoidal Nozzles

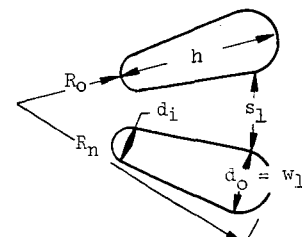
(a) Flat-ended

Number of elements	$D_e$ , cm	$D_{e,T}$ , cm	h, cm	$b_i$ , cm	$b_o$ , cm	$R_o$ , cm	$R_n$ , cm	$s_1/w_1$
12	2.18	7.55	3.15	0.86	1.56	3.07	6.3	1.15
6	3.14	7.70	3.15	1.61	3.30	3.00	6.2	1.01
6	3.19	7.80	5.23	0.90	2.16	3.06	8.4	3.06



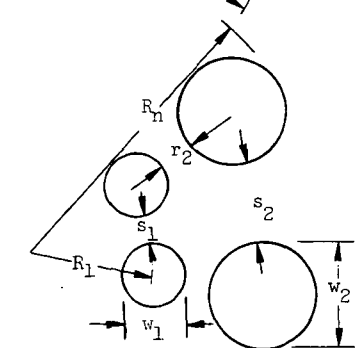
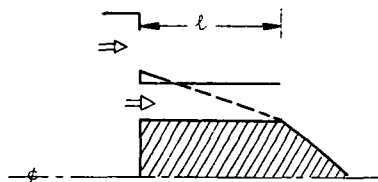
(b) Round-ended

8	3.81	10.8	6.25	1.19	2.51	2.59	8.8	1.37
---	------	------	------	------	------	------	-----	------



Noncoplanar Nozzles

Number of elements	$D_e$ , cm	$R_1$ , cm	$R_n$ , cm	$l$ , cm	$s_1/w_1$	$s_2/w_2$	$r_2/w_1$			
Core	8	1.41	2.54	4.06	8	10.2	1.25	1.01	0.445	
Bypass	3	8	2.36	2.54	2.54	8	10.2	0.85	1.01	0.71



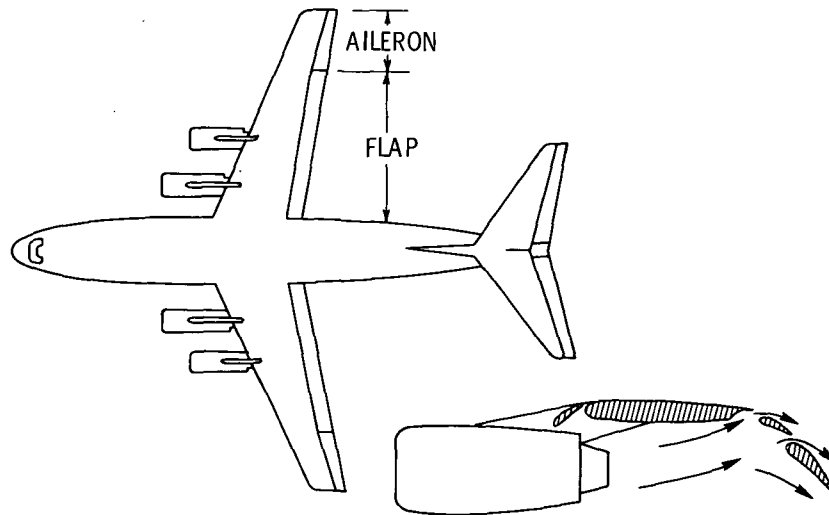


Figure 1. - Externally-blown-flap STOL airplane.

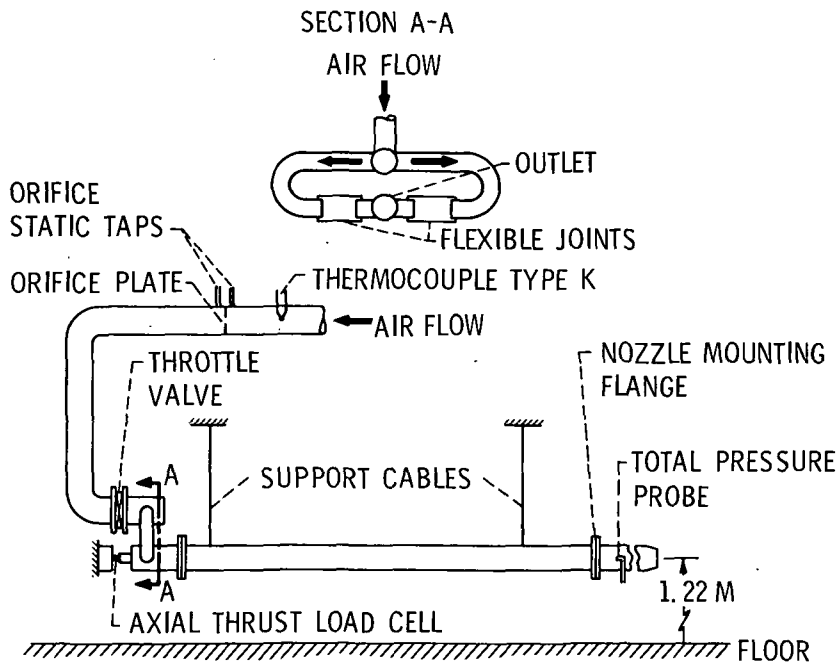


Figure 2. - Schematic diagram of test rig.

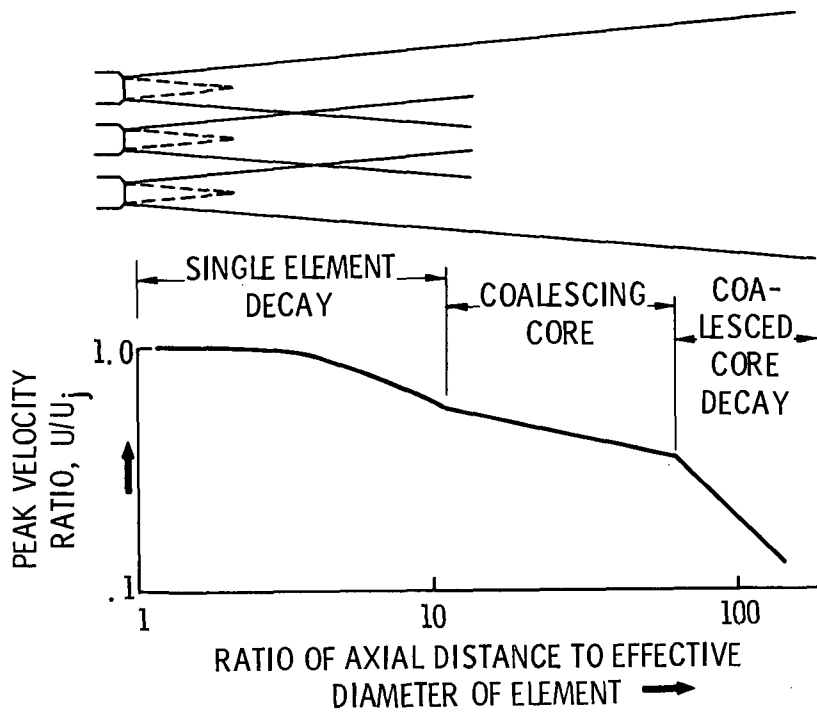
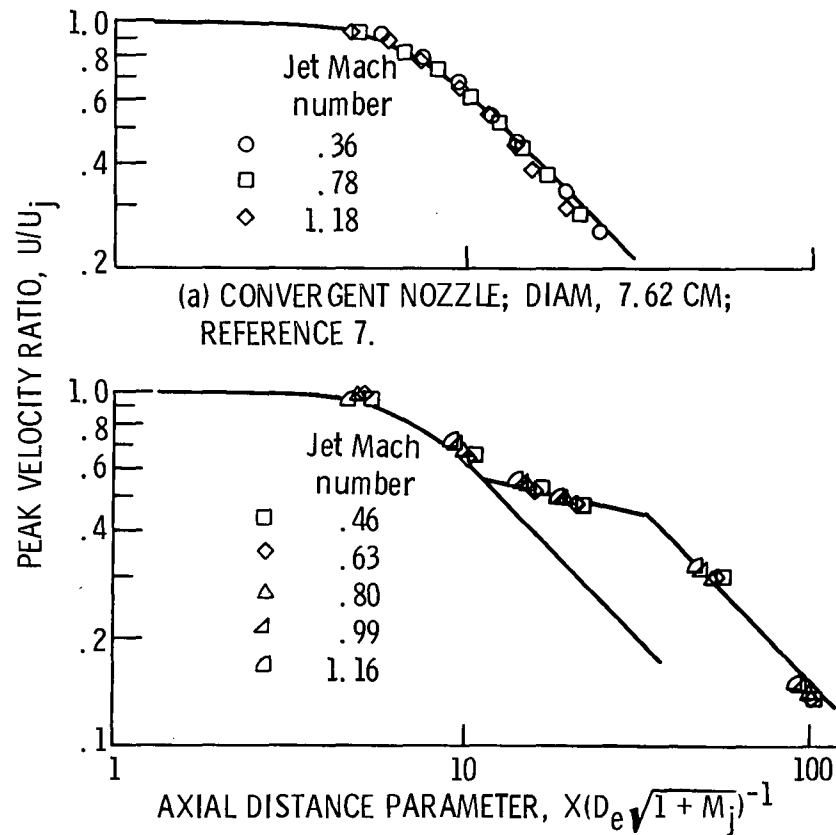


Figure 3. - Schematic of multi-element nozzle peak axial-velocity decay.



(b) 6-TUBE NOZZLE; TUBE DIAM, 2.36 CM; CIRCUMFERENTIAL TUBE SPACING, 2.7 CM.

Figure 4. - Typical peak axial-velocity decay obtained at various jet Mach numbers with single- and multi-element nozzles.

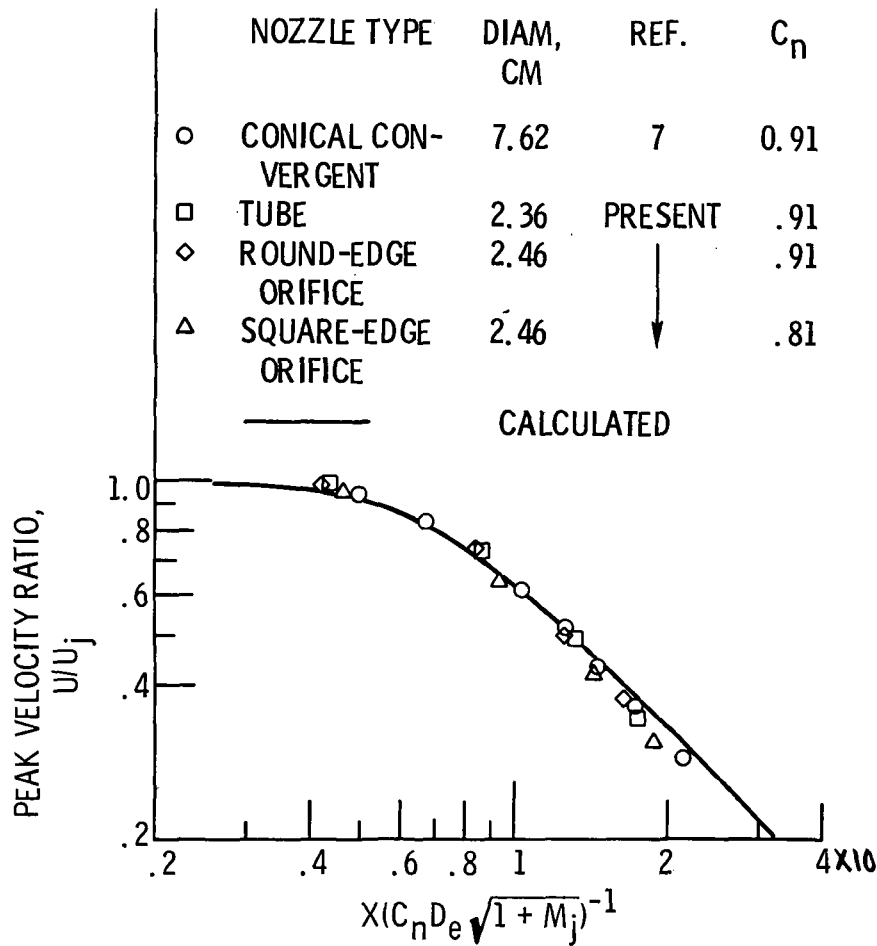


Figure 5. - Peak axial-velocity decay obtained with circular nozzles. Nominal jet Mach number, 0.8.

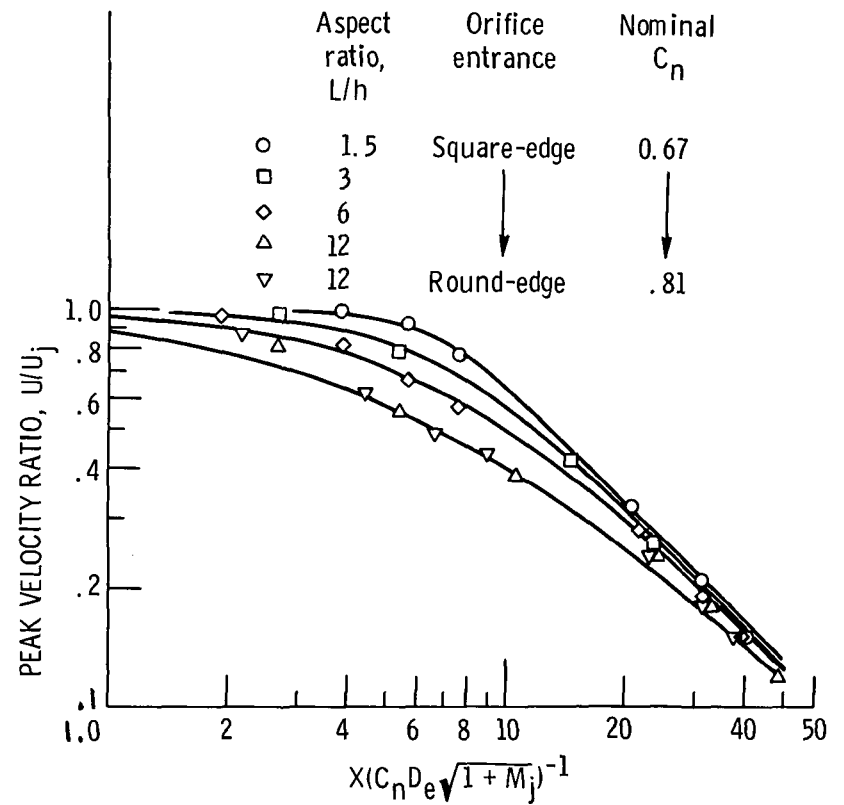
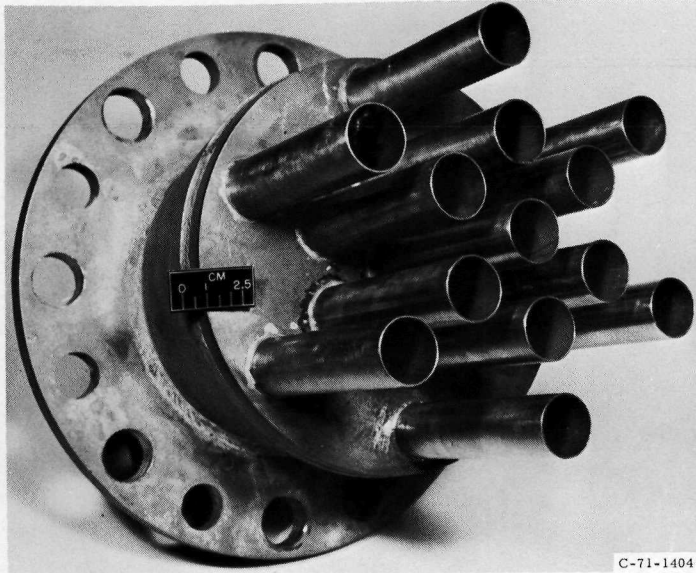
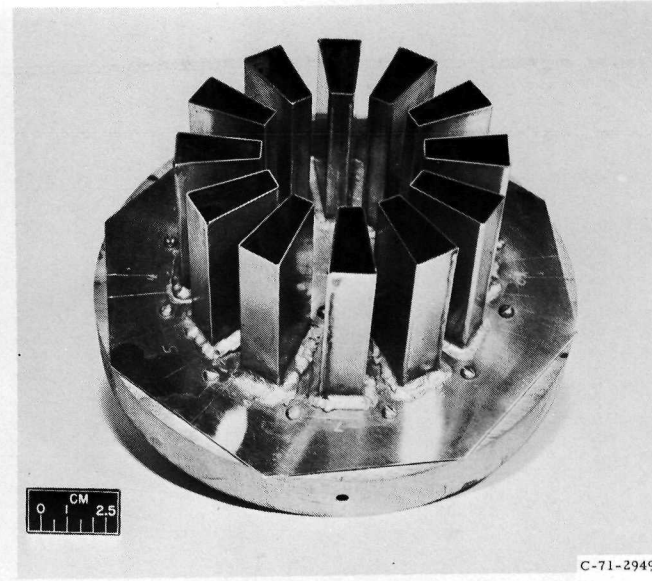


Figure 6. - Peak axial-velocity decay obtained with rectangular orifice-type nozzles.



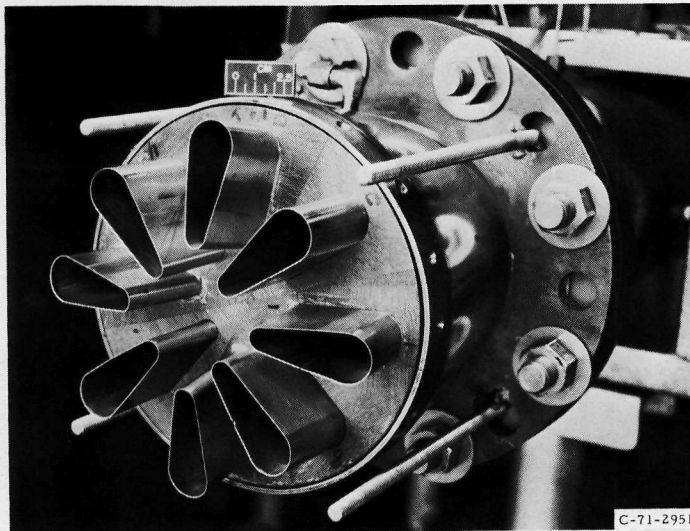
C-71-1404

(a) MULTITUBE NOZZLE.



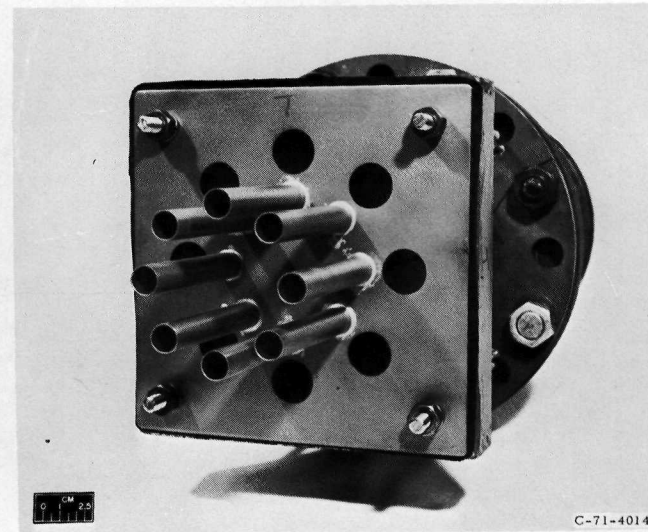
C-71-2949

(b) FLAT-ENDED TRAPEZOIDAL NOZZLE.



C-71-2951

(c) ROUND-ENDED TRAPEZOIDAL NOZZLE. ALTERNATE LOBES CANTED  $10^\circ$  OUTWARD FROM NOZZLE CENTERLINE.



C-71-4014

(d) BYPASS-TYPE NOZZLE WITH 8 CORE TUBES AND 8 SECONDARY-FLOW ORIFICES.

Figure 7. - Typical multi-element nozzles.



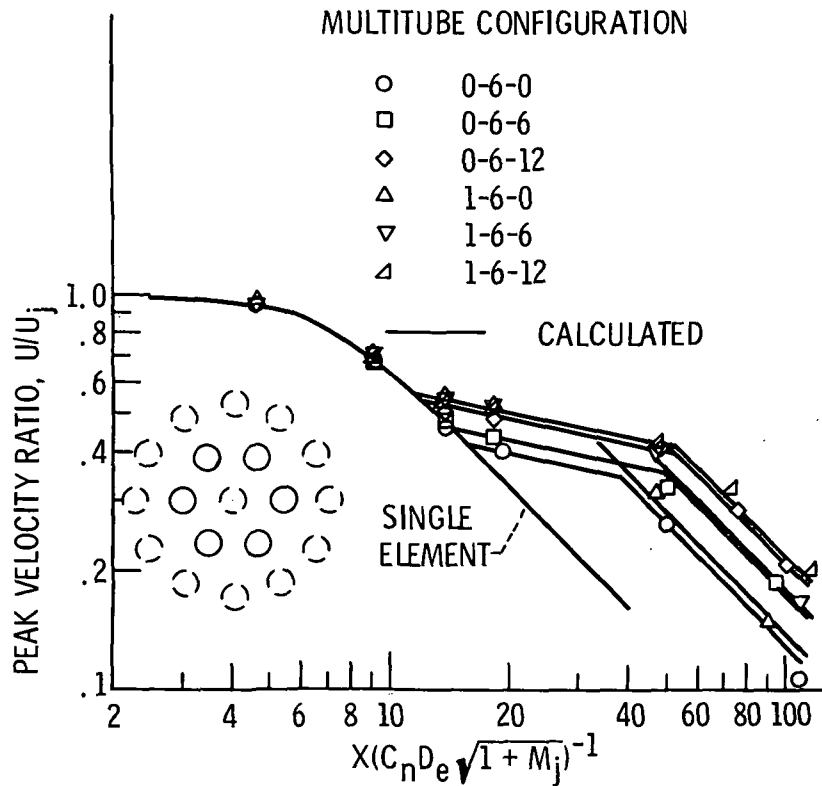


Figure 10. - Effect of center tube and/or multi-rings of tubes on peak axial-velocity decay of multitube nozzles. Nominal  $C_n$ , 0.828;  $s_1/w_1 = r_1/w_1 = r_2/w_1$ .

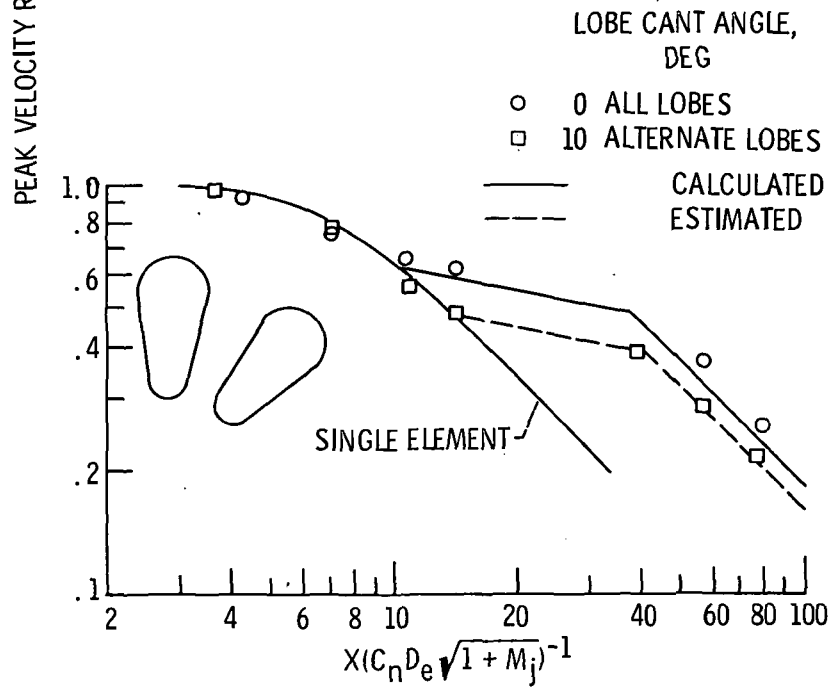
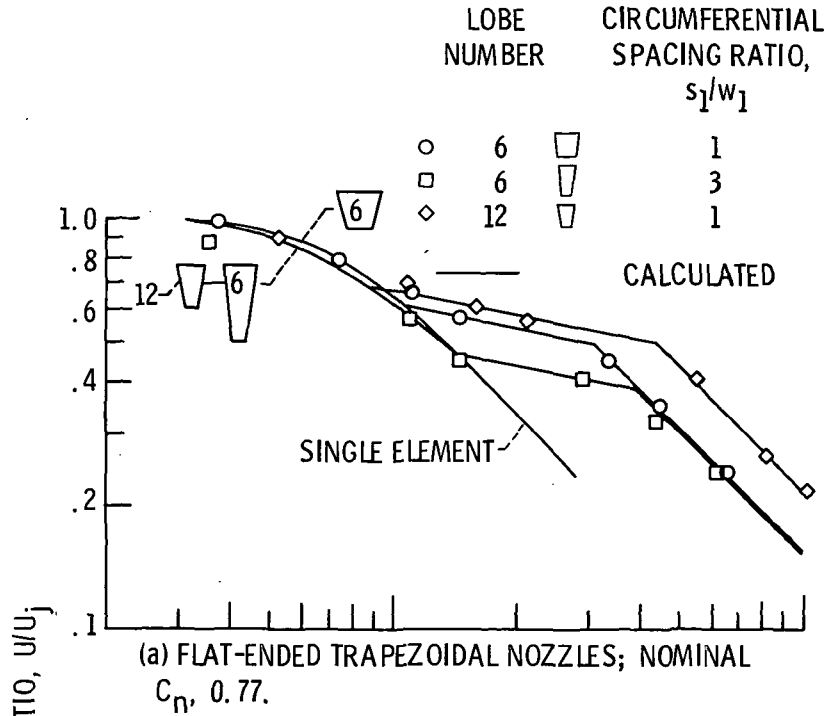


Figure 11. - Peak axial-velocity decay obtained with trapezoidal multi-element nozzles.

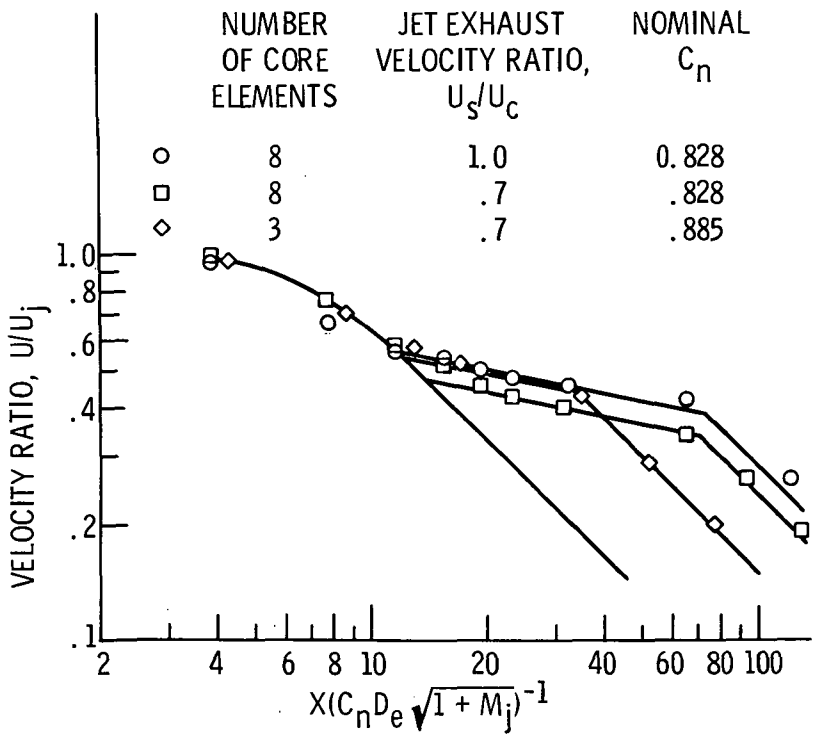


Figure 12. - Typical peak-axial velocity decay for non-coplanar multi-element nozzles. Secondary nozzle, 8-circular orifices.

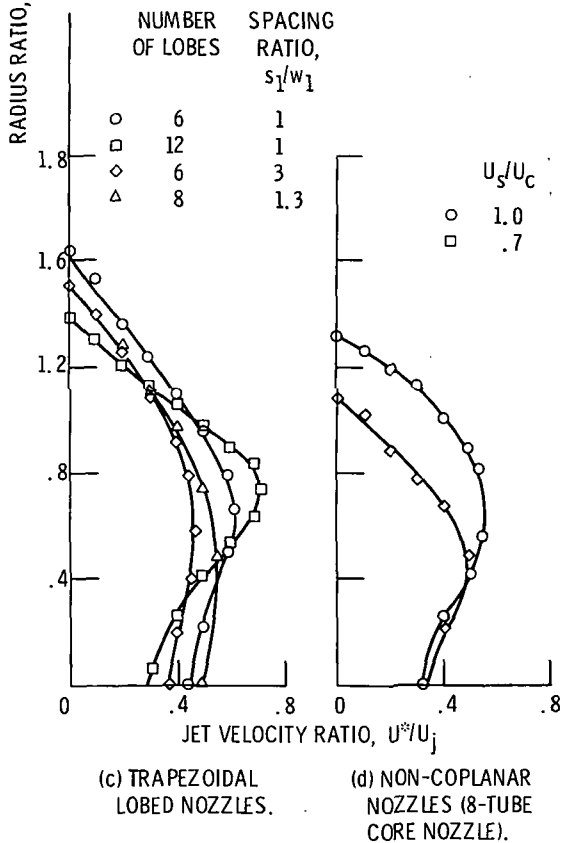
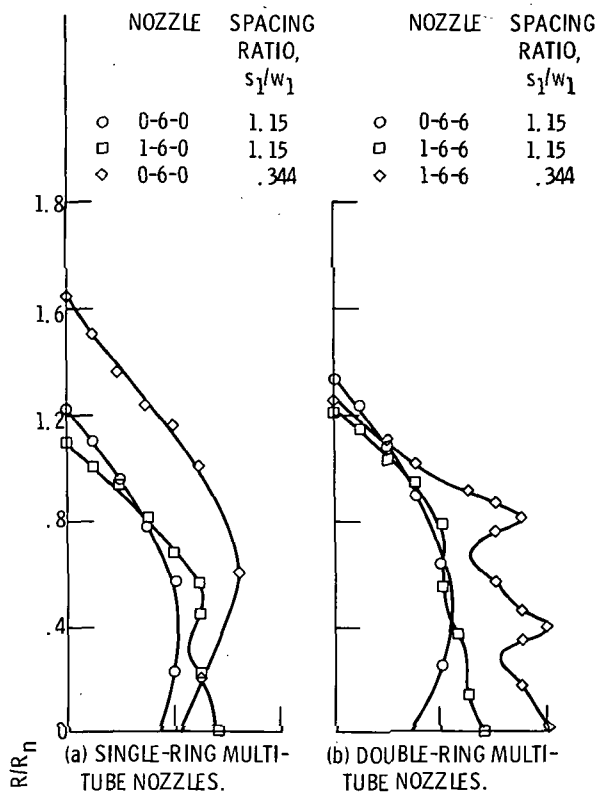
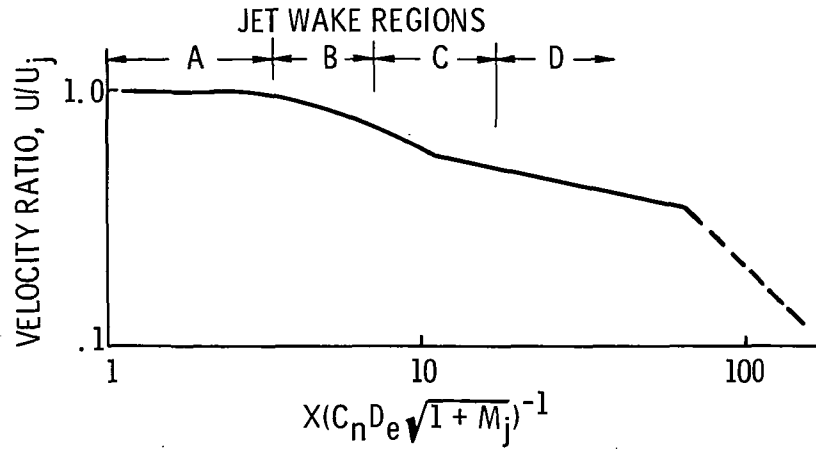


Figure 13. - Typical radial profiles of jet velocities at departure point of coalescing core from single-element decay curve.



AVERAGE JET SPREADING HALF-ANGLE, DEG				
NOZZLE TYPE	JET WAKE REGION			
	A	B	C	D
MULTITUBES				
SINGLE RING	6±1	2-3	6	5
DOUBLE RING	7±1	1	6±1	5
TRAPEZOIDAL LOBES	8±1	3-4	6	4±1
NON-COPLANAR				
$U_s/U_c, 1.0$	---	2	4	3
$U_s/U_c, 0.7$	---	3	5	4

Figure 14. - Relation of jet-wake spreading half-angle to velocity decay.